Chemomechanical assessment of beams damaged by alkali-silica reaction

Stéphane Multon, Jean-François Seignol, Francois Toutlemonde

Chemo-mechanical assessment of beams damaged by Alkali-Silica Reaction

Stéphane Multon[1], Jean-François Seignol[2], François Toutlemonde[3]

Manuscript number: **MT/2004/022869**

Abstract

The Alkali-Silica Reaction (ASR) is a chemical reaction which causes expansions and unexpected deformations of concrete structures. A methodology of assessment of ASR-damaged structures is required in order to evaluate their structural stability. Chemo-mechanical calculations have been performed in order to investigate the assumption of modeling ASR-induced expansions as imposed strains. The input data for the model comprises of the moisture distribution in the damaged structures, ASR-induced potential strains and the influence of ASR on the concrete mechanical properties. The results of calculations have been compared with the experimental data obtained from ASR-damaged beam specimens. The role of water supply and reinforcement have been analyzed in comparing the deformations of plain and reinforced concrete beams subjected to a moisture gradient. Calculations show that cracking and compressive stresses (here induced by steel reinforcement) have a large influence on the anisotropy of the ASR-swellings. This induced anisotropy is shown to be one of the main factors which should be considered while predicting the mechanical behavior of ASR-damaged structures.

[1] Ph.D, Grad. Teacher, Dept of Civ. Engrg. INSA / LMDC, 135, ave de Rangueil, 31077 Toulouse Cedex, France. E-mail: multon@insa-toulouse.fr

[2] Ph.D, Res. Engi., LCPC, 58, bld Lefebvre, 75732 Paris, Cedex 15, France. E-mail: seignol@lcpc.fr

[3] Head of Struct. Lab., Ph.D., Pr. Res. Eng., LCPC, 58, bld Lefebvre, 75732 Paris, Cedex 15, France. E-mail: toutlemo@lcpc.fr

Introduction

A significant number of civil engineering structures (bridges, road pavements, dams, etc) are damaged by the Alkali-Silica Reaction (ASR). This chemical reaction between alkalis and certain siliceous aggregate, containing reactive particles, causes expansions in concrete, large cracking and deformations of structures. Determining the consequences of such a reaction is of great practical significance for the owners of ASR-damaged civil engineering structures. The magnitude and the time-evolution of ASR induced strains depend on: reactive compound content (alkali and reactive silica), environmental conditions (temperature, Relative Humidity (Olafsson, 1986), water supply (Larive, 1998), (Larive *et al.*, 2000-a) and stress conditions due either to mechanical loading (Larive *et al.*, 1996), (Gravel *et al.*, 2000), (Multon, 2004), (Multon *et al.*, 2004) or to restraint of ASR expansion provided by the steel reinforcement (Swamy and Al-Asali, 1990), (Fan and Hanson, 1998), (Monette *et al.*, 2002), (Multon *et al.*, 2005). Moreover, ASR-expansions appear to be highly anisotropic depending on the casting direction (Clark, 1991), (Larive, 1998), (Larive *et al.*, 2000-b), (Smaoui, 2003). The consequences of ASR on concrete mechanical properties are still debated and appear to be different depending on the nature of reactive aggregate. Some authors observed a decrease in all the mechanical properties (Pleau *et al.*, 1989), (Smaoui, 2003) while other concrete mixtures exhibited mostly a decrease in the Young's modulus (Larive, 1998), (Monette *et al.*, 2002). Models developed to predict the structural behavior of such damaged structures (Ulm *et al.*, 2000), (Li and Coussy, 2002), (Capra and Sellier, 2003) take into account most of these phenomena. However the ASR-anisotropy and the effect of stresses on ASR-expansions are not still perfectly described by these predictive models.

The aim of the present research was to investigate the possibility of modeling ASR-expansions as imposed strains, which depend on concrete mix-design and environmental conditions as described in the thermo-hydro-chemo mechanical model developed by (Ulm *et*

al., 2000) and (Li and Coussy, 2002). In this approach, the required external input data are the temperature and the moisture conditions (determined by *in situ* measurements). The ASR-induced strains are computed knowing the potential expansion due to concrete mix-design (measured by residual expansion tests (Bérubé *et al.*, 2002)). The merits of this method is the simplicity in obtaining the input data. The thermo-hydro calculations use already validated models (Maingy *et al.*, 1999). The aim of this paper is to validate the chemo-mechanical part of the structural assessment method according to chemo-elastic calculations based on the Strength of Materials assumptions, by comparison with experimental data obtained on damaged beams in (Multon, 2004), (Multon *et al.*, 2005). The effects of water supply and reinforcement on ASR-induced strains have been studied both experimentally and numerically, focusing on induced expansion anisotropy.

Chemo-elastic approach

Parameters

Temperature has an accelerating effect on ASR-expansion, but it does not affect the range of expansion. The effects on kinetics can be modeled by Arrhenius law (Larive, 1998), (Ulm *et al.*, 2000). Since the effect of temperature has already been studied (Ulm *et al.*, 2000), it was not chosen as a parameter for this study.

The effect of water supply on the range of ASR-swellings is commonly known (Olafsson, 1986), (Larive *et al.*, 2000-a). Real structures are submitted to drying, resulting in moisture gradients, and differential water supply. Such conditions lead to differential expansions between the parts submitted to high moisture content and the parts submitted to drying. Models have to predict the significant consequences of such moisture gradients on the structural behavior of ASR-damaged structures. Moreover, compressive stresses appear to reduce ASR-expansions along the most compressed direction (Larive *et al.*, 1996), (Gravel *et al.*, 2000), (Multon, 2004), (Multon *et al.*, 2004). Compressive stresses can be caused by

mechanical loading of structure, or induced by the presence of steel reinforcement (Swamy and Al-Asali, 1990), (Fan and Hanson, 1998), (Monette *et al.*, 2002). The role of water supply and compressive stresses in ASR-expansion is investigated in this paper.

Experiments on reactive beams

An experimental program is used in this paper to validate calculations (Multon, 2004), (Multon *et al.*, 2005). These experimentations were carried out on 3 m long, 0.25 m thick and 0.50 m high simply supported beam specimens (with a 2.80 m span – Fig. 1). The beams were submitted to vertical moisture gradient obtained by original environmental conditions in order to study the effect of water on ASR-expansion. The lower parts of the beams were immersed in water while the upper faces were exposed to air at 30% RH (Fig. 1). The lateral faces were sealed using a watertight cover. This vertical moisture gradient led to strain gradients (with shrinkage in the upper part and large ASR-expansions in the bottom) and thus to flexural deflections. Both plain and reinforced concrete beams (using re-bars with a 500 MPa yield stress) were monitored in the program (Table 1). All the specimens were exposed to a constant 38°C environment for about one year, leading to significant expansions after some months.

Modeling methodology

Since temperature was kept constant, calculations are based on three input variables: the water distribution in the structures, the potential ASR-induced strains (depending on moisture conditions) and the (possibly time dependent) concrete mechanical properties. The distribution of ASR induced strains in the whole structure was determined by using the first two input data. This distribution of chemical strains can be used as initial imposed strains in the equations of strength of materials (equilibrium of plane cross-sections) to predict the behavior of the three reactive beams. Experimental measurements provide for the input data: water distribution was measured on the beams, potential ASR-induced strains were obtained

on companion standard specimens and the evolution of mechanical properties was characterized at different times. Experimental results also provide for the strains and deflections necessary to validate models.

Input data

Imposed strains depend on moisture distribution in the damaged structures and on the response of reactive concrete to these local moisture conditions.

Moisture distribution in the ASR damaged beams

Water movements in the beams were produced by the environmental boundary shown in Fig. 1. Moisture distribution can be described by profiles of mass variations (Fig. 2) as follows: mass increase due to water absorption in the bottom of the beams; mass variations lower than the accuracy of the measurement device and hence assumed as null in the middle part of the beam; and mass loss due to drying in the upper 140 mm, measured using a gammadensitometry device (Multon and Toutlemonde, 2004), (Multon *et al.*, 2005). The profiles of mass variation were obtained considering the penetration of water in the bottom part of the beam as an idealized imbibition front propagating as the square root of time as described in (Hall, 1989), with a mean sorptivity S of about 6.10^{-3} m.day$^{-1/2}$.

ASR-induced potential expansion

Following (Larive *et al.*, 2000-a) in using the mass variations due to water supply as the influent parameter, Fig. 3 shows the mass variation and the strains of the concrete mixture under three moisture conditions at 38°C: in water, sealed under watertight aluminum cover and in air at 30% RH. Shrinkage is observed for large mass losses and expansion for mass increase or mass losses lower than 1%. Therefore, it has been assumed in the following calculations that shrinkage occurred for concrete with mass losses higher than 1% and ASR expansions occurred for concrete with mass losses lower than 1%. It can be observed in Fig. 3 that the larger the water supply, the larger the ASR-induced expansions, as already shown in

(Larive *et al.*, 2000-a). These expansions measured on specimens have been directly used in the following calculations as explained below.

Expansion measurements presented in Fig. 3 were performed on six specimens, cast from the same batch and stored in the same environment. The standard deviation (Fig. 3) is still high in spite of the similarity of the specimens. This can be explained by the heterogeneous repartition of the reactive silica inside the limestone aggregate (Larive, 1998), (Larive *et al.*, 2000-b). Moreover, the measurements were carried out along two perpendicular directions relative to the casting direction. The ASR-expansions showed anisotropy; expansions along the casting direction were twice as large as along the perpendicular direction (Clark, 1991), (Larive, 1998), (Larive *et al.*, 2000-b), (Smaoui, 2003).

Imposed strains distribution

Imposed strains distribution in the beams (Fig. 4) is determined by combining the input data on the moisture distribution (Fig. 2) and ASR-induced potential expansion (Fig. 3) as described below:

- ASR-induced strains $\boldsymbol{\varepsilon_{wat}}$ are measured on specimens kept in water. They are representative for concrete within the immersed part, or reached by the water penetration

$$z_{wat} \le z < h \qquad \Rightarrow \varepsilon_{imp}(t,z) = \varepsilon_{wat}(t) \tag{1}$$

where $z_{wat} = h - \left(0.07 + S\sqrt{t}\right)$ represents the depth of imbibition front.

- ASR-expansions $\boldsymbol{\varepsilon_{\delta m=0}}$ are representative for concrete without mass variation and are obtained from measurements on specimens kept in water and under aluminum. The expansions are calculated by assuming proportionality between ASR-expansions and mass variations (Larive, 1998), (Larive *et al.*, 2000-a). Fig. 5 shows how to obtain the following equation to calculate the imposed strain in concrete without mass variation.

$$z_d \le z < z_{wat} \qquad \Rightarrow \varepsilon_{imp}(t,z) = \varepsilon_{\delta m=0}(t) = \varepsilon_{wat}(t) - \frac{\varepsilon_{wat}(t) - \varepsilon_{seal}(t)}{\left.\frac{\delta m}{m}\right|_{wat}(t) - \left.\frac{\delta m}{m}\right|_{seal}(t)} \tag{2}$$

- ASR-expansions ε_{seal} measured on sealed specimens are used for concrete with mass losses lower than 1% as explained above,

$$z_{shr} \le z < z_d \qquad \Rightarrow \varepsilon_{imp}(t,z) = \varepsilon_{seal}(t) \tag{3}$$

- The profile of imposed strains is assumed to be linear with the depth for concrete with mass losses higher than 1% (Fig. 4). Shrinkage at the upper face ε_{shr} is taken proportional to the mass variation (Torrenti *et al*, 1999) and equal to zero at z_{shr} (depth where the mass variation is equal to –1%). The relationship between mass losses and shrinkage was deduced from measurement performed on specimens kept in air at 30% RH presented in Fig. 3:

$$\varepsilon_{shr}\left(\frac{\delta m}{m}\right) = 0.013\frac{\delta m}{m} + 0.007 \tag{4}$$

The equation of the straight line representing the shrinkage strain (Fig. 4) can be deduced from the drying depth z_{shr} (obtained in Fig. 2) and drying shrinkage $\varepsilon_{shr}\left(\frac{\delta m}{m}\right)$ (Eq. 4):

$$0.0 \le z < z_{shr} \qquad \Rightarrow \varepsilon_{imp}\left(\frac{\delta m}{m}\right) = \varepsilon_{shr}\left(\frac{\delta m}{m}\right)\frac{(-z + z_{shr})}{z_{shr}} \tag{5}$$

In this part, the shrinkage induced strains are considered as imposed strains.

Mechanical properties

Mechanical properties were measured at five time-steps during the experimental program (Multon, 2004), (Multon *et al.*, 2005). Compressive and tensile strengths had the same evolution as for non reactive concrete, as already observed in (Larive, 1998), (Monette *et al.*, 2002) with compressive and splitting tensile strengths of about 38 MPa and 3 MPa. The concrete Young's modulus at 28 days after casting is equal to 37,300 MPa. It is constant during the first 60 days of exposure. It decreases of about 20% between 60 and 150 days, and

stays equal to 30,100 MPa during the following year (Multon, 2004), (Multon *et al.*, 2005). The reduction can be explained by the initiation of ASR-cracks. Predictive models should take into account the decrease in Young's modulus.

Chemo-elastic calculation

Longitudinal strain measurements carried out on the beams show that the plane cross-sections remained plane during the whole experiment as shown in Fig. 6 for the beam B1, and reported for the three beams in (Multon, 2004), (Multon *et al.*, 2005). Thus, the beams fulfill Navier-Bernoulli's assumption, and calculations according to Strength of Materials hypotheses can be used.

Strength of Materials

Chemo-elastic calculations have been performed to predict the flexural behavior of the ASR-damaged beams. Strains due to self-weight of the structures (about 5 µm/m) can be neglected compared to shrinkage and chemically induced strains (between 500 and 2500 µm/m). Equations of equilibrium of plane cross-sections for reinforced concrete beams are:

$$\begin{cases} N(t) = \int_0^h \sigma(t,z).b.dz + A\sigma_s(t,d) + A'\sigma_s(t,d') = 0 \\ M_f(t) = \int_0^h \sigma(t,z).z.b.dz + dA\sigma_s(t,d) + d'A'\sigma_s(t,d') = 0 \end{cases} \quad (6)$$

with A, A', d, d' given in Table 1.

Shrinkage and ASR-induced strains are assumed to be imposed strains. In the elastic range, the chemo-elastic concrete constitutive law reads:

$$\sigma(t,z) = E_c(t).(\varepsilon(t,z) - \varepsilon_{imp}(t,z)) \quad (7)$$

E_c stands for concrete equivalent Young's modulus for long term calculations.

For long term calculations, it is necessary to take into consideration the delayed strains due to concrete creep. The ratio between delayed and instantaneous strains for this concrete

mixture was estimated about 3 (determination from long term loaded specimens (Multon, 2004), (Multon *et al.*, 2004)). An equivalent long term Young's modulus can be obtained by dividing by 4 the "instantaneous" Young's modulus measured on specimens.

Since plane cross-sections remained plane during the whole experiment, longitudinal strains read:

$$\varepsilon(t,z) = \varepsilon'_0(t).z + \varepsilon_0(t) \tag{8}$$

where $\varepsilon'_0(t)$ and $\varepsilon_0(t)$ are two unknown variables. Assuming perfect bond between concrete and the reinforcement steel, stress in the lower (Eq. 9) and upper reinforcing bars read (Eq. 10):

$$\sigma_s(t;d) = E_s(\varepsilon'_0\, d + \varepsilon_0) \text{ and } \sigma_s(t;d') = E_s(\varepsilon'_0\, d' + \varepsilon_0) \tag{9), (10}$$

with E_s = 200000 MPa.

At each time-step, the system (11) derives from equations (6) to (10) (with $n = E_s / E_c$):

$$\begin{cases} \varepsilon'_0\left(\frac{h^2}{2} + \frac{n}{b}(dA + d'A')\right) + \varepsilon_0\left(h + \frac{n}{b}(A + A')\right) = \int_0^h \varepsilon_{imp}(z).dz = I_N \\ \varepsilon'_0\left(\frac{h^3}{3} + \frac{n}{b}\left(d^2A + d'^2\,A'\right)\right) + \varepsilon_0\left(\frac{h^2}{2} + \frac{n}{b}(dA + d'A')\right) = \int_0^h \varepsilon_{imp}(z).z.dz = I_M \end{cases} \tag{11}$$

where I_N and I_M derive from equations (1) to (4):

$$\begin{cases} I_N = \varepsilon_{wat}(h - z_{wat}) + \varepsilon_{\delta m=0}(z_{wat} - z_d) + \varepsilon_{seal}(z_d - z_{shr}) + \frac{z_{shr}.\varepsilon_{shr}}{2} \\ I_M = \frac{\varepsilon_{wat}}{2}(h^2 - z_{wat}^2) + \frac{\varepsilon_{\delta m=0}}{2}(z_{wat}^2 - z_d^2) + \frac{\varepsilon_{seal}}{2}(z_d^2 - z_{shr}^2) + \frac{z_{shr}^2.\varepsilon_{shr}}{6} \end{cases} \tag{12}$$

where z_d is the depth of the drying front (m), z_{shr}, the depth along which shrinkage occurred (m), and z_{wat}, the depth reached by the water penetration (m).

The system (11) has been numerically solved for every time-step, and thus structural behavior of the ASR-damaged beams have been predicted from the input data (moisture distribution, ASR-induced potential expansion and mechanical evolution of concrete). Since the cross-sections remained plane during the whole experiment, the longitudinal behavior of

the beams can be described by only two variables, for instance, by the longitudinal strain at the depth of 0.23 m and the mid-span deflection. These experimental data can be compared to the calculated ones:

$$\varepsilon(0.23) = 0.23.\varepsilon'_0 + \varepsilon_0 \text{ and } d_{ms} = \varepsilon'_0 . \frac{l^2}{8} \qquad (13), (14)$$

Accuracy of calculations

Uncertainty of the calculations results from uncertainty concerning the moisture distribution and from the large scatter in the ASR-induced strains measured on specimens. For the depth of the drying front z_d, accuracy is related to the resolution of the gammadensitometry device (u_{zd} = 0.01 m). For the depth of water penetration z_{wat}, accuracy is related to uncertainty of the sorptivity S ($u_S = 1.5 \times 10^{-3}$ m.day$^{-1/2}$). For the ASR-induced strains, the heterogeneity of ASR-expansion is significantly larger than the measurement accuracy. Accuracy can be taken equal to the standard deviation of shrinkage and ASR induced strain values measured on specimens (Fig. 3). Uncertainty of the calculations can thus be estimated by derivation of the formulae corresponding to solving the system (11). For the strains at the depth of 0.23 m, it reads:

$$u_{\varepsilon(z)} = \sqrt{\left(\frac{\partial \varepsilon(z)}{\partial \varepsilon_{wat}} u_{wat}\right)^2 + \left(\frac{\partial \varepsilon(z)}{\partial \varepsilon_{\delta m=0}} u_{\delta m=0}\right)^2 + \left(\frac{\partial \varepsilon(z)}{\partial \varepsilon_{shr}} u_{shr}\right)^2 + \left(\frac{\partial \varepsilon(z)}{\partial S} u_S\right)^2 + \left(\frac{\partial \varepsilon(z)}{\partial z_d} u_{zd}\right)^2} \qquad (15)$$

The same calculation can be carried out for the mid-span deflection. This uncertainty is represented as the half-height of the interval around the computed value in Fig. 7, 9, 11 and 13.

Structural assessment of the plain concrete beam

Calculation 1: Effect of casting direction on anisotropy

The anisotropy of ASR-expansions is commonly observed relative to the casting direction (Clark, 1991), (Larive, 1998), (Larive *et al.*, 2000-b), (Smaoui, 2003). For the beams, the longitudinal direction was perpendicular to the casting direction. The system (12) has been

solved for the plain concrete beam (A = A' = 0) with the assumption that ASR-induced strains were equal to the strains measured on specimens perpendicular to the casting direction. The predicted values of mean strain and mid-span deflection show a good agreement with the measurements performed on the beam during the first 150 days (Fig. 7). The structural behavior after this period is not correctly predicted. It had to be noted that cracking of the beam was observed on the immersed part 160 days after the beginning of measurement (Fig. 8). The initiation of cracking of the immersed face can be considered as predicted by the chemo-mechanical calculations, since tensile stresses calculated in the lower part of the beam reach 4 MPa after 150 days. The equation (7) should not be used in the cracked concrete. Cracks caused discontinuities in concrete and thus a reduction of the section of the beam. Preliminary calculations had been carried out to calculate the height of the cracked part and thus to determine the reduction of the section of the beam. However, observations showed that cracks were filled by ASR-gel. The ASR-gel kept on swelling and pushed on the two faces of cracks. Preliminary calculations which did not consider the cracked part also neglected the ASR-expansions in this part, and did not lead to satisfactory agreement in the computing post-cracking evolution. After these preliminary calculations, it was assumed that equation (7) could be used in spite of cracking. This computation is shown in Calculation 2.

Calculation 2: Effect of cracking on anisotropy

ASR-induced cracking of specimens is mainly perpendicular to casting direction and the larger ASR-expansions have always been measured perpendicular to cracks (Clark, 1991), (Larive, 1998), (Larive *et al.*, 2000-b). This can be explained by the intrinsic anisotropy of concrete which would favor the opening of horizontal cracks. The formation of ASR-gels would then be favored in these horizontal cracks, which would cause larger expansions along the direction perpendicular to cracks (Larive, 1998), (Larive *et al.*, 2000-b). Observations on the present beam prove that most of the cracks were in transverse direction (Fig. 8). Larger

ASR-imposed strains could have occurred along the cracked part of the beam. New calculations have thus been performed with the assumption that imposed strains were equal to strains measured on specimens perpendicular to casting direction in the whole beam, except in the cracked part. In this part, imposed strains have been taken equal to the largest strains (measured along the casting direction). The effect of cracking is thus included in the calculation by considering the anisotropy of ASR-expansions induced by the initiation of cracks. Since cracks were first observed after 160 days and reached a depth between 0.04 m and 0.10 m at 425 days, a linear time evolution of the cracked height has been assumed to carry out the calculations between 150 days and 425 days first, with a final cracked height of 0.04 m (Calculation 2-a), then with a final cracked height of 0.10 m (Calculation 2-b). The stiffness is modified following the evolution of measured Young's modulus described below. Calculations taking into account the effect of cracking on ASR-anisotropy show better agreement, especially with respect to mid-span deflection (Fig. 7-b). This illustrates that ASR models should consider this phenomenon. However, the mean strain was hardly better predicted (Fig. 7-a), and further assumptions were studied.

Calculation 3: Isotropy for concrete without cracking

Taking into account the effect of cracking on ASR-anisotropy, it appears to be more realistic to consider isotropic expansion in the part of the beam where little cracking takes place, and larger expansion in the cracked part. The isotropic potential expansion has been evaluated from the strains measured on specimens (Fig. 3) as reported in (Seignol *et al.*, 2004):

$$\varepsilon_{iso} = \frac{\varepsilon_{cast\_dir} + 2\varepsilon_{perp}}{3} \tag{15}$$

where ε_{cast_dir} is the ASR-expansion measured along the casting direction and ε_{perp} is the expansion measured perpendicularly to the casting direction.

The ASR-imposed strains have been taken equal to isotropic expansion in the whole beam except in the cracked part. In the cracked part, imposed strains have been taken equal to the strains measured on specimens along the casting direction. A linear time evolution of the cracked height has been still assumed between 150 days and 425 days with a final depth of cracking equal to 0.04 m (which was measured along the main part of the cross-section). It allows good predictions to be obtained (Fig. 9) especially after 250 days. However the predicted structural behavior in the first 200 days is worse than the previous calculations.

Discussion 1 (plain concrete beam)

Previous assumptions and calculations show that the anisotropy measured on specimens can not be used directly for structural calculations. However, the complex effects of cracking on ASR-anisotropy should be considered in order to predict the mechanical behavior of ASR-damaged structures. Calculation 3 is consistent with observations performed on the beam. Indeed, it predicts tensile stresses higher than 3 MPa after 50 days, which explains the transverse cracks observed on the upper face during the experiment (Multon *et al.*, 2005). It also predicts the cracking of the lower face with tensile stresses higher than 4 MPa in the bottom of the beam after 150 days. However, even if the structural behavior can be simulated, the accuracy relative to the computed deflection is about 0.70 mm for a 5.2 mm deflection (about 15%) mainly due to the scatter in the ASR-expansion.

Structural assessment of the reinforced concrete beams

Numerous papers have emphasized the reduction of observed ASR-induced strains due to reinforcing bars (Swamy and Al-Asali, 1990), (Fan and Hanson, 1998), (Monette *et al.*, 2002). In this part of the paper, the effect of reinforcing steel on the structural behavior of the ASR-damaged reinforced beams is investigated and analyzed following the same Strength of Materials methodology.

Effect of the cracking direction on ASR-anisotropy

The previous calculations have shown the influence of cracking direction on ASR-anisotropy in structures. In order to assess the structural behavior of the tested reinforced concrete beams, two calculations have been carried out:

a) The first calculation assumes that ASR-expansion in the beam is isotropic. Only the elastic effect of the steel reinforcement is considered.

b) The second calculation takes into account the effect of cracking direction on ASR imposed strains. For the reinforced beams, cracking was mainly longitudinal (Fig. 10). Imposed strains have been taken equal to the average isotropic value in the whole beam except in the (bottom) cracked part. In this part, imposed strains have been taken equal to ASR-expansions measured perpendicular to casting direction (and thus parallel to cracking direction). Cracks appeared at 90 and 200 days for B3 and B4, respectively and reached maximum depths estimated at 0.12 m and 0.15 m. A linear time evolution of the depth of cracking has been assumed between the initiation of cracks and the 425^{th} day, when deformations were stabilized.

The system of equation (11) has been solved for the reinforced beam B3 (with A, d, A' and d' in Table 1). The calculations show a bad prediction of its structural behavior (Fig. 11), particularly for the mid-span deflection, even if the effect of cracking on ASR-anisotropy is taken into consideration. The structural behavior of the reinforced beams can thus not be explained only by the elastic effect of reinforcing bars. A large decrease of the imposed strains in the lower part of the beam appeared as a necessary cause of the observed behavior. It could be explained by the effect of the compressive stresses around the reinforcing bars.

Effect of compressive stresses on ASR-induced anisotropy

Calculations of the stresses along the height of the beam (Equation 7) show that two parts were subjected to significant compressions: the immersed concrete, close to the lower reinforcing bars, and concrete at mid-height (Fig. 12). In the lower part, the compressive

stresses were caused by the confinement of ASR-expansions due to reinforcing steels. Whatever the imposed strains, calculated compressive stresses were higher than 5 MPa after about 50 days close to the reinforcing bars. Compressive stresses in the intermediate zone are mainly explained by the assumed discontinuous profile of imposed strains close to z_d. In reality, the imposed strains should be more continuous in this part. It could cause a diminution of these compressive stresses. Moreover, this zone is smaller than the first one. Therefore, the compressive stresses in the concrete at mid-height are neglected in subsequent calculation. While unsatisfactory for predictive calculations, it allows the effect of compression stresses on structural behavior of ASR-damaged beams to be investigated.

Compressive stresses higher than 5 MPa may largely reduce ASR-expansions along the compressed direction due either to mechanical loading (Larive *et al.*, 1996), (Gravel *et al.*, 2000), (Multon, 2004), (Multon *et al.*, 2004) or to restraint of ASR expansion by steel reinforcement (Swamy and Al-Asali, 1990), (Fan and Hanson, 1998), (Monette *et al.*, 2002), (Multon *et al.*, 2005). ASR expansions are not only counteracted by the compressive stresses, they appear to be largely prevented in the compressed directions. Therefore, ASR-induced strains had been assumed to be significantly reduced in the compressed part. In order to assess simply the structural behavior of the reinforced concrete beams, a reduction factor (α) has been affected on the ASR imposed strains in the immersed part, Equation 1 was changed in:

$$\boldsymbol{h} - \left(0.07 + \boldsymbol{S}\sqrt{\boldsymbol{t}}\right) \leq \boldsymbol{z} < \boldsymbol{h} \qquad \Rightarrow \varepsilon_{imp}(t,z) = \alpha.\varepsilon_{wat}(t) \tag{16}$$

This reduction factor has been determined for each beam to minimize the quadratic deviation between calculated and measured strains at 0.23 m of depth and mid-span deflections. These calculations finally show good agreement with the measurements using a reduction factor of 0.45 and 0.30 for B3 and B4 respectively (standard deviation of about 0.005% for the strain and 0.100 mm for the deflection – Fig. 13). It suggests that the compressive stresses caused decrease of ASR-imposed strains of about 55% and 70%. The stresses in the reinforcing steels

could be estimated to 160 MPa and 100 MPa for B3 and B4 respectively. This estimation appears as realistic, even if it could not be compared to direct measures. It confirms that significant ASR-induced stresses in the steel reinforcement should be accounted for in assessment of ASR-damaged structures.

Discussion 2 (reinforced concrete beam)

As for the plain concrete beam, these calculations cannot be considered as predictive, since the behavior had to be known to determine the reduction factor. The analysis proves that steel reinforcement has not only a direct effect of "prestressing" the beams by restraining the expansions; the compressive stresses due to local restraint by steels cause a reduction of ASR-induced expansion along the compressed direction. Reduction may reach 50% even for a 0.45% reinforcement ratio (B3). The accuracy relative to the computed deflections lies between 0.5 mm and 0.7 mm for deflections of about 1.1 mm and 0.3 mm. This accuracy is mainly due to the heterogeneity of measured ASR-expansions. The resulting scatter of calculated data is quite constant for all calculations (about 0.6 mm). For the plain concrete beam, it is only 15% of the measured deflection but for the reinforced beams, it is between 60 and 200% of the deflections measured on the beams. This effect of ASR-heterogeneity on predictive calculations should not be ignored.

Finally, it is suggested that an isotropic ASR-induced strain could be taken as a basic input data. This "isotropic" data must be obtained by averaging the strains measured along the three directions of standard specimens, for instance it may account for axial and transverse expansions of cylinders. It should then be multiplied by a factor, corresponding either to a reduction (compressive stresses reduce ASR-induced strains along the compressed direction) or to an increase (tensile stresses induce cracks which increase ASR-expansion perpendicularly to cracking direction). This factor is related to the local stress state, and structural assessments would be possible if it can be determined. An approach is to try to

determine the law linking the real ASR-anisotropy in concrete to the local stress state. An attempt of direct experimental insight in determining this anisotropy factor, only depending of the stress deviator, is given in (Multon, 2004) – obtained values appear as consistent with fitted determinations of α (0.3 to 0.5) obtained in the present paper. Obviously, further investigations are still necessary to validate such methods.

Conclusions

The concrete mixture, the environmental conditions, the potential water supply and the stresses due to both mechanical loading and reinforced-induced restraint of ASR-expansions are major parameters to be considered while predicting the mechanical behavior of ASR-damaged structures.

Predictive models using chemo-elasticity concepts have not still solved how to take into consideration the effect of compressive stresses on ASR-expansions. The development of concrete cracking, the compressive stresses and the effect of ASR-induced strains on the stresses within structures modify the directions of further ASR-induced expansions and thus the ASR-anisotropy. Therefore, iterative calculations appear to be necessary.

This paper proposes some modeling strategies to make predictive calculations. Finally, whatever the approach, ASR-modeling should take into consideration the effects of both cracking and compressive stresses on ASR-anisotropy for predicting the behavior of ASR-damaged structures.

Acknowledgements

The authors are pleased to thank S. Prené, H. Tournier, E. Bourdarot, A. Jeanpierre and D. Chauvel (EDF) for their help in analysis. They also thank particularly B. Godart and T. Kretz (LCPC) for their ideas of investigation.

Appendix. References

Bérubé, M.-A., Duchesne, J., Dorion, J.F., and Rivest, M. (2002), "Laboratory assessment of alkali contribution by aggregates to concrete and application to concrete structures affected by alkali-silica reactivity," *Cem. Conc. Res.*, 32(8), 1215-1227.

Capra, B., and Sellier, A. (2003), "Orthotropic modelling of alkali-aggregate reaction in concrete structures: numerical simulations," *Mech. Mat.*, 35(8), 817-830.

Clark, L.A. (1991), "Modeling the structural effects of Alkali-Aggregate Reaction on reinforced concrete," *Mat. J.*, ACI, 88(3), 271-277.

Fan S., and Hanson J.M. (1998), "Length expansion and cracking of plain and reinforced concrete prisms due to Alkali-Silica Reaction", *Struct. J.*, ACI, 95(4), 1998-a, 480-487.

Gravel, C., Ballivy, G., Khayat, K., Quirion, M., and Lachemi, M. (2000), "Expansion of AAR concrete under triaxial stresses : simulation with instrumented concrete block," *Proc., 11th Int. Conf. AAR*, Centre de Recherche Interuniversitaire sur le Béton, Quebec, Canada, 949-958.

Hall, C. (1989), "Water sorptivity of mortars and concretes : a review," *Mag. Conc. Res.*, 41(147), 51-61.

Larive, C., Laplaud, A., and Joly, M. (1996), "Behavior of AAR-affected concrete: Experimental data", *Proc. of 10th Int. Conf. AAR*, A. Shayan ed., Melbourne, Australia, 670-677.

Larive, C. (1998), "Apports combinés de l'expérimentation et de la modélisation à la compréhension de l'alcali-réaction et de ses effets mécaniques", PhD Thesis, Ecole Nationale des Ponts et Chaussées (France), Report OA 28, ERLPC Collection, Laboratoire Central des Ponts et Chaussées, Paris (in French).

Larive, C., Laplaud, A., and Coussy, O. (2000-a), "The Role of Water in Alkali-Silica Reaction", *Proc. of 11th Int. Conf. AAR,* Centre de Recherche Interuniversitaire sur le Béton, Quebec, Canada, 61-70.

Larive, C., Joly, M., and Coussy, O. (2000-b), "Heterogeneity and anisotropy in ASR-affected concrete - Consequences for structural assessment", *Proc. of 11th Int. Conf. AAR,* Centre de Recherche Interuniversitaire sur le Béton, Quebec, Canada, 969-978.

Li, K., and Coussy, O. (2002), "Concrete ASR degradation: from material modeling to structure assessment", *Conc. Sc. and Eng.*, RILEM, 4(13), 35-46.

Mainguy, M., Coussy, O., and Eymard, R. (1999), *Modélisation des transferts hydriques isothermes en milieu poreux. Application au séchage des matériaux à base de ciment*, Report OA 32, ERLPC Collection, Laboratoire Central des Ponts et Chaussées, Paris (in French).

Monette, L.J., Gardner, N.J., and Grattan-Bellew, P.E. (2002), "Residual strength of reinforced concrete beams damaged by Alkali-Silica Reaction - Examination of damage rating index method", *Mat. J.*, ACI, 99(1), 42-50.

Multon, S. (2004), "Evaluation expérimentale et théorique des effets de l'alcali-réaction sur des structures modèles", PhD thesis, Université de Marne la Vallée (France), Report OA 46, ERLPC Collection, Laboratoire Central des Ponts et Chaussées, Paris (in French).

Multon, S., and Toutlemonde, F. (2004), "Water distribution in concrete beams", *Mat. Struct.*, RILEM, 37(270), 378-386.

Multon, S., Leclainche, G., Bourdarot, E, and Toutlemonde, F. (2004), "Alkali-Silica Reaction in specimens under multi-axial mechanical stresses", *Proc., CONSEC'04*, B.H. Oh *et al.* (eds), Seoul Nat. Univ, Seoul, Korea, 2004-2011.

Multon, S., Seignol J-F., and Toutlemonde, F. (2005), "Structural behavior of concrete beams affected by ASR", *Mat. J.*, ACI, 102(2), 67-76.

Pleau, R., Bérubé, M.A., Pigeon M., Fournier, B., and Raphael, S. (1989), "Mechanical behavior of concrete affected by ASR", *Proc., 8th Int. Conf. AAR,* Elsevier Applied Science Publishers Ltd (England), Kyoto, Japan, 721-726.

Olafsson, H. (1986), "The effect of relative humidity and temperature on alkali expansion of mortar bars," *Proc., 7th Int. Conf. AAR,* Noyes Publication (New Jersey – USA), Ottawa, Canada, 461-465.

Seignol, J-F., Barbier, F., Multon, S., and Toutlemonde, F. (2004), "Numerical simulation of ASR affected beams, comparison to experimental data", *Proc. 12th Int. Conf. AAR,* Int. Academic Publishers, Beijing World Publishing Corp., Beijing, China, 198-206.

Smaoui, N. (2003), "Contribution à l'évaluation du comportement structural des ouvrages d'art affectés de réaction alcali-silice (RAS)," PhD thesis, Faculté des Sciences et de Génie de l'Université de Laval, Québec, Canada (in French).

Swamy, R.N., and Al-Asali, M.M. (1990), "Control of Alkali-Silica Reaction in reinforced concrete beams", *Mat. J.,* ACI, 87(1), 38-46.

Torrenti, J.-M., Granger, L., Diruy, M., Genin, P. (1999), "Modeling concrete shrinkage under variable ambient conditions", *Mat. J.,* ACI, 96(1), 35-39.

Ulm, F.-J., Coussy, O., Li, K., and Larive, C. (2000), "Thermo-Chemo-Mechanics of ASR expansion in concrete structures," *J. Engrg. Mech.,* ASCE, 126(3), 233-242.

Appendix. Notation

A	area of lower steel reinforcement (m²)
A'	area of upper steel reinforcement (m²)
b	beams thickness (m)
d	distance between the center of gravity of the lower steel reinforcement and the upper face of the beam (m)

d'	distance between the center of gravity of the upper steel reinforcement and the upper face of the beam (m)
d_{ms}	mid-span deflection of beam (m)
E_c	Equivalent long term Young's modulus for concrete (MPa)
E_s	Young's modulus of steel reinforcement (MPa)
h	height of beam (m)
l	span of beam (m)
M_b	bending moment (MN.m)
n	Young's modulus ratio (E_s / E_c)
N	axial force (N)
S	sorptivity (m.day$^{-1/2}$)
t	time (day)
z	depth along the height of the beams (m)
z_d	depth of the drying front (m)
z_{shr}	depth along which shrinkage occurred (m)
z_{wat}	depth reached by the water penetration (m)
α	reduction factor multiplying ASR-imposed strains due to compressive stresses
$\delta m/m$	relative mass variation
ε	strain
ε_{imp}	imposed strain
ε_s	steel strain
σ	stress (MPa)
σ_s	steel stress (MPa)

Table 1. Characteristics of the three ASR-damaged beams

Beams	Lower Reinforcement	Upper reinforcement
B1	**None**	**None**
B3	**2 ribbed #16 bars (d = 0.450 m)**	**2 ribbed #10 bars (d' = 0.045 m)**
B4	**2 ribbed #32 bars (d = 0.420 m)**	**2 ribbed #20 bars (d' = 0.050 m)**

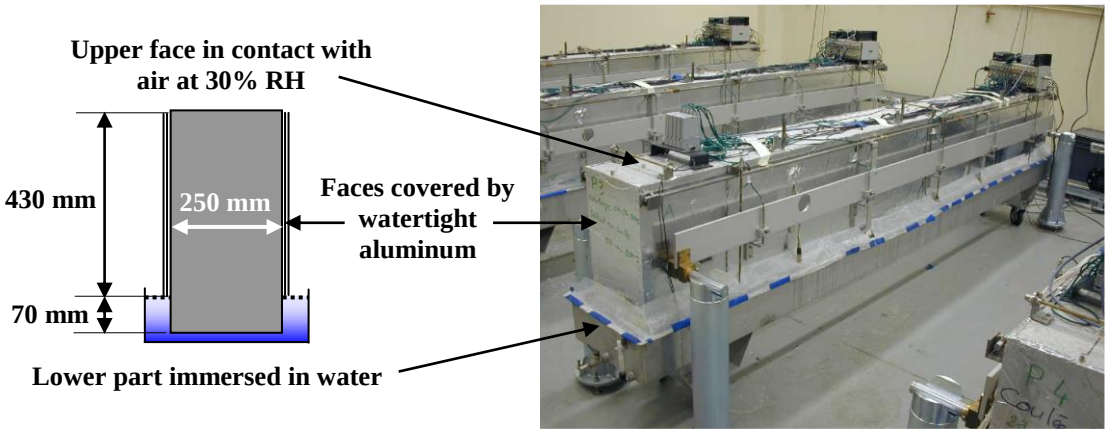

Fig. 1. Environmental conditions of the three beams

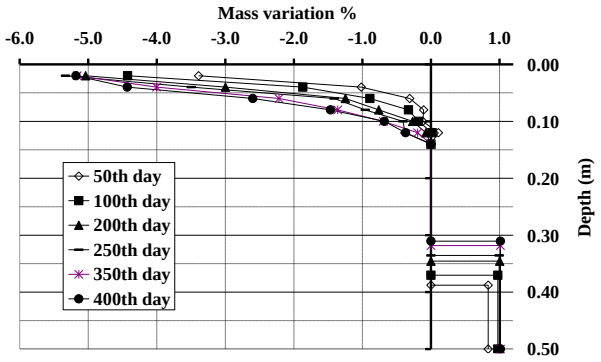

Fig. 2. Profiles of mass variation along the height of the beams

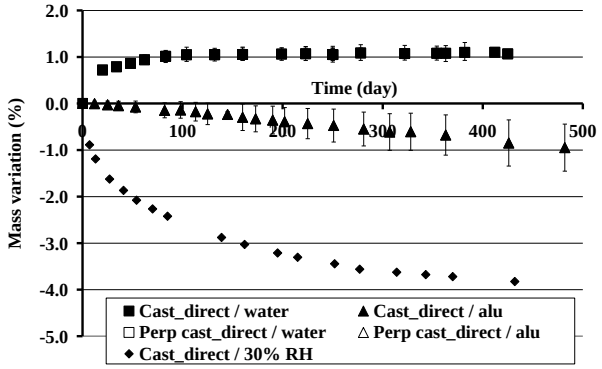

(a)

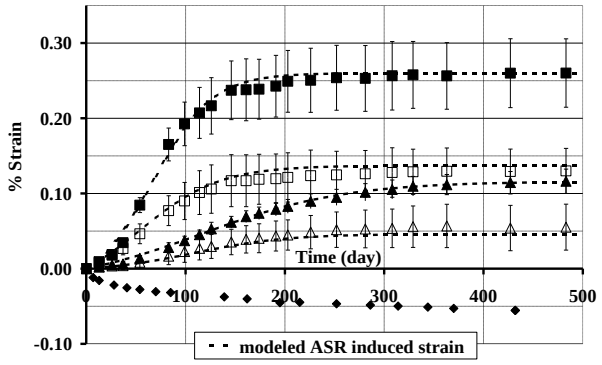

(b)

Fig. 3. Mass variation (a) and potential expansion (b) of reactive concrete

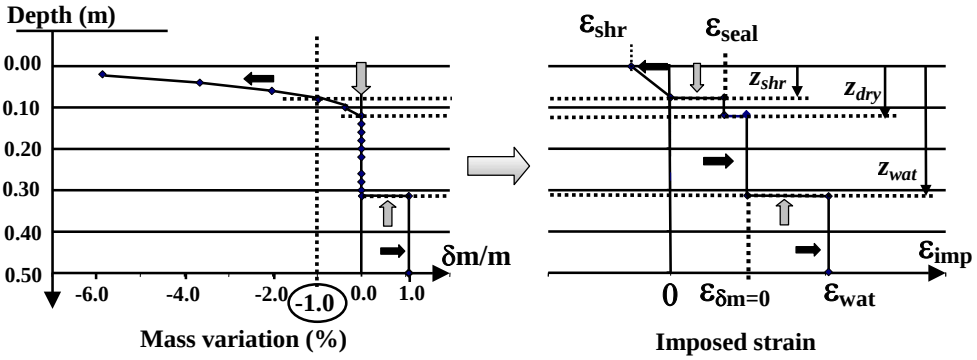

Fig. 4. Profile of imposed strains along the height of the beams

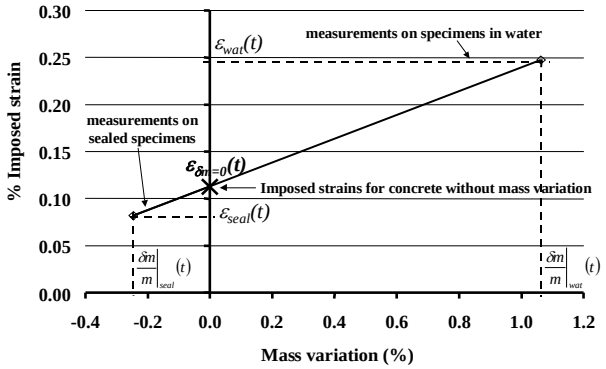

Fig. 5. Imposed strains interpolated from measurements on specimens kept in water and under aluminum for concrete without mass variation

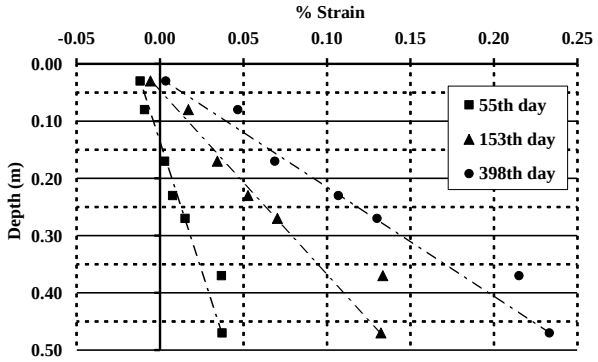

Fig. 6. Plane cross-sections of the plain concrete beam (B1) during the experiment

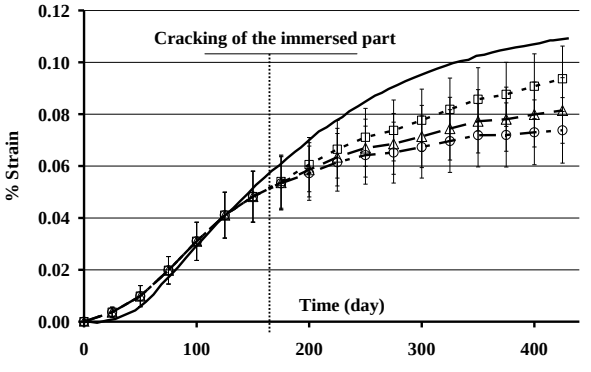

(a)

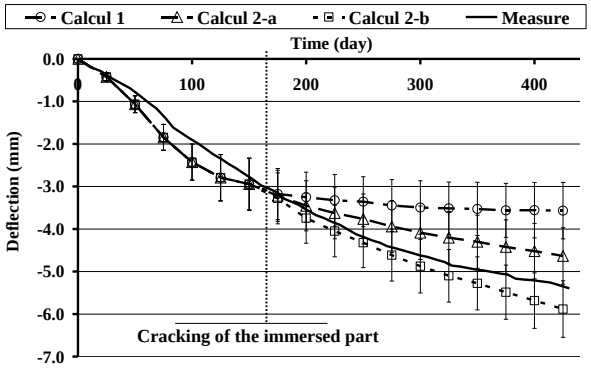

(b)

Fig. 7. Measured and calculated strain at the depth of 0.23 m (a) and mid-span deflection (b) of the plain concrete beam (B1) assuming that anisotropy depends on casting direction (Calculation 1) and taking into account the effect of cracking direction on anisotropy (Calculation 2-a and 2-b)

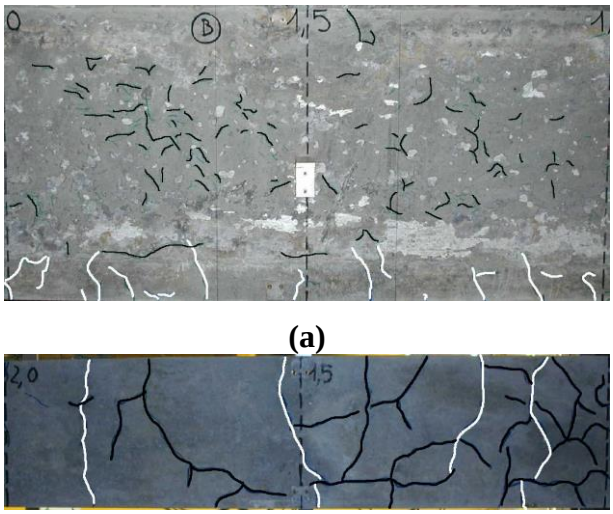

(a)

(b)

Fig. 8. Cracking of the plain concrete and reactive beam (B1), central 1 m-part: (a) lateral face, (b) lower immersed face

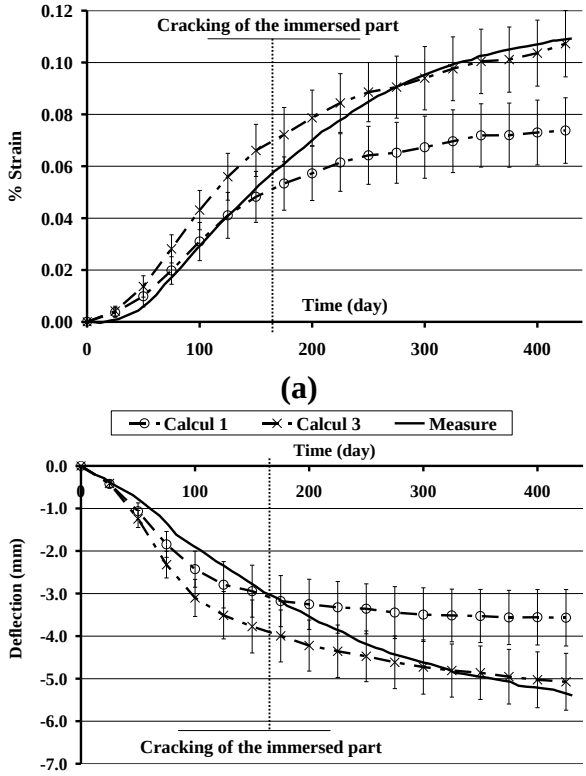

Fig. 9. Measured and calculated strain at the depth of 0.23 m (a) and mid-span deflection (b) of the plain concrete beam B1 taking into account isotropic expansion in the whole beam except in the cracked part

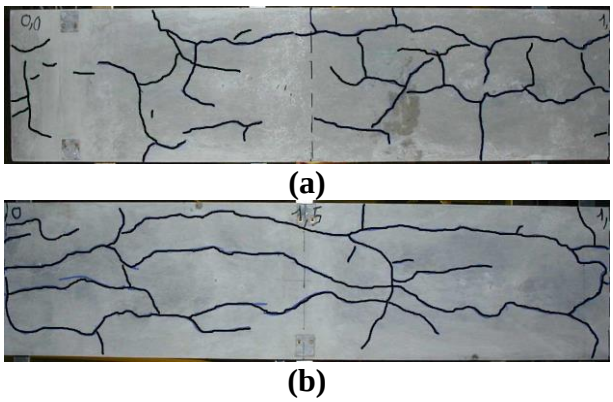

Fig. 10. Cracking of the reinforced and reactive beam (B3), central 1 m-part: (a) lateral face, (b) lower immersed face

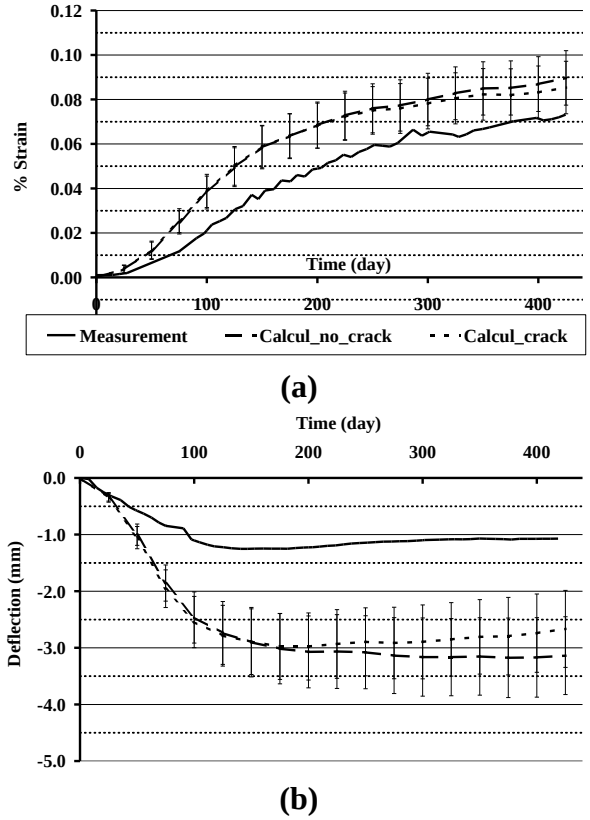

Fig. 11. Measured and calculated strain at the depth of 0.23 m (a) and mid-span deflection (b) of the reinforced and reactive beam (B3)

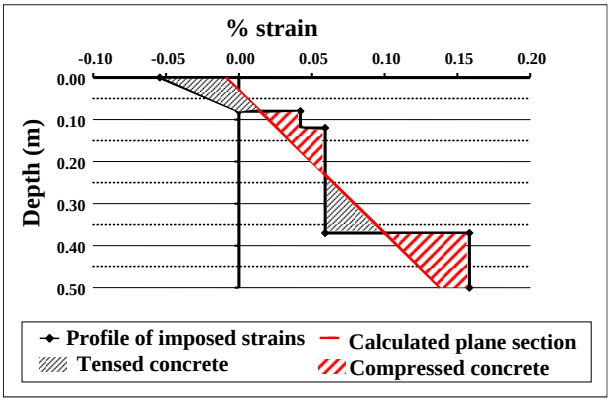

Fig. 12. Profile of imposed strains and plane cross section at 150 days for the reinforced and reactive beam (B3)

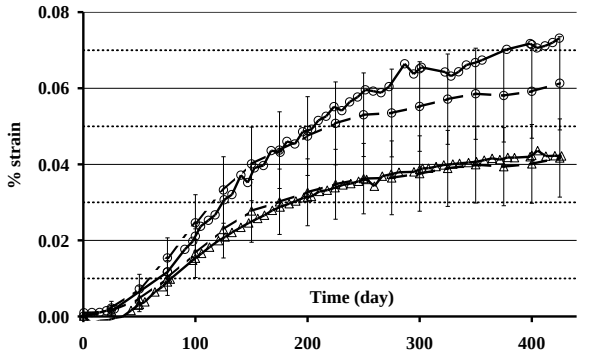

(a)

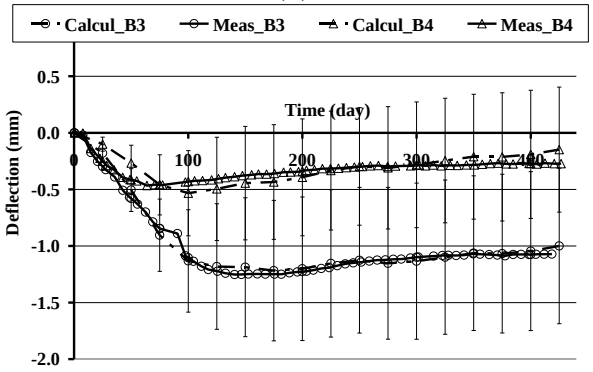

(b)

Fig. 13. Measured and calculated strain at the depth of 0.23 m (a) and mid-span deflection (b) of the two reinforced and reactive beams (B3, B4) taking into account the effect of compressive stresses

List of figure captions:

Fig. 1. Environmental conditions of the three beams

Fig. 2. Profiles of mass variation along the height of the beams

Fig. 3. Mass variation (a) and potential expansion (b) of reactive concrete

Fig. 4. Profile of imposed strains along the height of the beams

Fig. 5. Imposed strains interpolated from measurements on specimens kept in water and under aluminum for concrete without mass variation

Fig. 6. Plane cross-sections of the plain concrete beam (B1) during the experiment

Fig. 7. Measured and calculated strain at the depth of 0.23 m (a) and mid-span deflection (b) of the plain concrete beam (B1) assuming that anisotropy depends on casting direction (Calculation 1) and taking into account the effect of cracking direction on anisotropy (Calculation 2-a and 2-b)

Fig. 8. Cracking of the plain concrete and reactive beam (B1), central 1 m-part: (a) lateral face, (b) lower immersed face

Fig. 9. Measured and calculated strain at the depth of 0.23 m (a) and mid-span deflection (b) of the plain concrete beam B1 taking into account isotropic expansion in the whole beam except in the cracked part

Fig. 10. Cracking of the reinforced and reactive beam (B3), central 1 m-part: (a) lateral face, (b) lower immersed face

Fig. 11. Measured and calculated strain at the depth of 0.23 m (a) and mid-span deflection (b) of the reinforced and reactive beam (B3)

Fig. 12. Profile of imposed strains and plane cross section at 150 days for the reinforced and reactive beam (B3)

Fig. 13. Measured and calculated strain at the depth of 0.23 m (a) and mid-span deflection (b) of the two reinforced and reactive beams (B3, B4) taking into account the effect of compressive stresses

Keywords

Alkali-Silica Reaction, Anisotropy, Chemo-Mechanical Modeling, Durability, Expansive concrete, Moisture gradient, Reinforced concrete, Structural assessment.